Climate Data Record (CDR) Program

Climate Algorithm Theoretical Basis Document (C-ATBD)

Polar Pathfinder FCDR

CDR Program Document Number: CDRP-ATBD-0572
Revision 3 / July 19, 2023
Configuration ID#: 01B-24a

REVISION HISTORY

Rev.	Author	DSR No.	Description	Date
1	Yinghui Liu, CIMSS UW-Madison; Jeff Key, NOAA; Andrew Heidinger, NOAA	DSR-734	Initial baseline submission to the CDR Program Library	09/16/2015
2	Yinghui Liu, Jeff Key, Xuanji Wang	DSR-1334	Final update for APP v2.0	02/07/2019
3	Xuanji Wang, Yinghui Liu, Jeff Key	DSR-1806	Final update for Polar Pathfinder FCDR v3.0	07/19/2023

TABLE of CONTENTS

LIST of FIGURES

LIST of TABLES

1. Introduction

1.1 Purpose

The purpose of this document is to describe the algorithm used to create the Polar Pathfinder Fundamental Climate Data Record (FCDR) from 1982 to the present. Polar Pathfinder FCDR uses the observations from the Advanced Very High Resolution Radiometer (AVHRR)/Visible Infrared Imaging Radiometer Suite (VIIRS) onboard the NOAA polar orbiting satellites. Its purpose is to provide calibrated and navigated sensor data for the generation of higher level geophysical parameters. In particular, it is the primary input to the eXtended AVHRR/VIIRS Polar Pathfinder Product, APP-x/VPP-x. APP-x/VPP-x is described in a separate C-ATBD. The algorithm is defined by the computer program (code) that accompanies this document. The purpose of this document is to provide an understanding the data processing algorithm, from both a scientific perspective, and to assist a software engineer or end-user performing an evaluation of the code or the data.

1.2 Definitions

The following is a summary of the symbols used to define the algorithm.

Instrument count related parameters:

C = *instrument count* (1)

C_0 = *dark or switch count* (2)

C_{rel} = *relative instrument count* (3)

Calibration slope-related parameters:

S = *calibration slope* (4)

S_0 = *calibration slope at launch* (5)

S_1 = *calibration parameter for* t (6)

S_2 = *calibration parameter for* t^2 (7)

t = *time in years since launch* (8)

BT = Brightness Temperature (9)

Reflectance related parameters:

R_u = *reflectance unadjusted for sun-earth distance or solar zenith angle* (10)

R = *reflectance adjusted for sun-earth distance and solar zenith angle* *(11)*

θ = *solar zenith angle* *(12)*

D_{se} = *sun-earth distance* *(13)*

PRT = Platinum Resistance Thermometer *(14)*

T_{PRT} = *blackbody temperature of the PRT* *(15)*

T_{BB} = *Internal blackbody temperature* *(16)*

SW = smoothing weight *(17)*

N_{BB} = *radiance for the internal blackbody* *(18)*

N_S = *radiance for the cold space* *(19)*

C_{BB} = *Mean count values of the internal blackbody* *(20)*

C_S = *Mean count values of the cold space* *(21)*

N_{LIN} = *Linear radiance estimate* *(22)*

N_{COR} = *Non linear correction of radiance* *(23)*

1.3 Document Maintenance

Table 1 defines the versions of the Polar Pathfinder FCDR CDR product release, the corresponding software package, and the C-ATBD. The Production software package is maintained at NCEI Subversion version control system.

Table 1. Versions of the Polar Pathfinder FCDR product release, software, and the C-ATBD.

Release Date	Product Version	Software Version	C-ATBD Version	Subversion Branch	Remarks
2015-09-01	V01	V01	V1.0	TBD	Initial draft
2019-01-15	V02	V02	V2.0		C-ATBD update
2023-07-19	V02	V03	V3.0		C-ATBD update

1.4 Improvements and VPP addition in APP

Version 2.0 of the APP fundamental climate data record has three important improvements: (1) the calibration uses the same code of the Clouds from AVHRR Extended (CLAVR-x) processing system and the AVHRR PATMOS-x (Pathfinder Atmosphere-Extended) calibration available at https://svn.ssec.wisc.edu/repos/cloud_team_clavrx/trunk/ (Foster and Heidinger 2013), with the latest calibration coefficients of May 2018 for improved accuracy and efficiency, (2) the entire data record (1982 – present) has been reprocessed for consistency, (3) the addition of VIIRS data, called VPP, starting from 2012 for current APP extension to the VIIRS era. One minor update is the reflectance channel calibration in section 3.4.1.1, solar-earth distance factor is included. In v1.0, we took the same calibration approach of CLAVR-x and PATMOS-x, but wrote our code in another computer language, and got very similar results as CLAVR-x and PATMOS-x except non-negligible differences in visible channel reflectance. While the changes in v2.0 are significant for the dataset, the foundation of the algorithm remains the same.

2. Observing Systems Overview

2.1 Products Generated

The Polar Pathfinder FCDR product is comprised of calibrated and navigated AVHRR/VIIRS channel data (reflectances of visible channels and brightness temperatures of thermal channels), viewing and illumination geometry (sensor scan angle, solar zenith angle, and sun-sensor relative azimuth angle), Universal Coordinated Time (UTC) of the data acquisition, and a surface type mask. The data includes twice-daily composites on a 5 km Equal-Area Scalable Earth (EASE)-Grid over both poles, the Arctic and Antarctic, from 1982 to the present. The daily Polar Pathfinder FCDR composites are centered on local solar times (LST) of 04:00 and 14:00 (high sun, but could be nighttime for some polar areas in winter) for the Arctic and 02:00 and 1400 for the Antarctic. The purpose of compositing based on local solar time rather than synoptic (UTC) time is to capture the diurnal cycle at all locations throughout the Arctic and Antarctic. Each composite is composed of as many as 23 orbits from the previous day to the next day (i.e. +/- 1 day), depending on the longitude of a pixel. Polar Pathfinder FCDR covers the north polar region (Arctic) from 48.4 degrees northward, and the south polar region (Antarctic) from -53.2 degrees southward.

2.2 Instrument Characteristics

The series of NOAA Polar Orbiting Environmental Satellites (POES) started with TIROS-N (launched in October 1978), and continued with NOAA-A (renamed NOAA-6), NOAA-C (NOAA-7), NOAA-E (NOAA-8), NOAA-F (NOAA-9), NOAA-G (NOAA-10), NOAA-H (NOAA-11), NOAA-D (NOAA-12), NOAA-I (NOAA-13), NOAA-J (NOAA-14), NOAA-K (NOAA-15), NOAA-L (NOAA-16), NOAA-M (NOAA-17), NOAA-N (NOAA-18), MetOp-A, NOAA-N' (NOAA-19), and MetOp-B (Table 2) (Kidwell et al. 1995, 2009). The continuity of the instrument payload onboard the NOAA POES series provide an uninterrupted flow of global environmental information for establishing long-term data sets for climate monitoring. The

Joint Polar Satellite System (JPSS) is the nation's advanced series of polar-orbiting environmental satellites with a new and sophisticated instrument called Visible Infrared Imaging Radiometer Suite (VIIRS) having more channels in place of previous AVHRR. The five satellites scheduled in the fleet are the currently-flying NOAA/NASA Suomi National Polar-orbiting Partnership (Suomi NPP) satellite, NOAA-20, previously known as JPSS-1, NOAA-21, previously known as JPSS-2, and the upcoming JPSS-3 and JPSS-4 satellites. Table 2 provides some basic details associated with each of the NOAA POES series.

Table 2: NOAA POES series

Satellite Number	Launch Date	Ascending Node[1]	Descending Node	Service Date[2]
TIROS-N	10/13/78	1500	0300	10/19/78 – 1/30/80
NOAA-6	06/27/79	1930	0730	06/27/79 – 1/16/86
NOAA-7	06/23/81	1430	0230	08/24/81 – 2/01/85
NOAA-8	03/28/83	1930	0730	05/03/83 – 0/31/85
NOAA-9	12/12/84	1420	0220	02/25/85 – 1/07/88
NOAA-10	09/17/86	1930	0730	11/17/86 – 9/16/91
NOAA-11	09/24/88	1340	0140	11/08/88 – 6/16/04
NOAA-12	05/14/91	1930	0730	09/17/91 – 8/10/07
NOAA-14	12/30/94	1340	0140	04/10/95 – 5/23/07
NOAA-15	5/13/98	1930	0730	12/15/98 - present
NOAA-16	09/21/00	1400	0200	03/20/01 - present
NOAA-17	06/24/02	2200	1000	10/15/02 - 4/10/13
NOAA-18	05/20/05	1400	0200	08/30/05 - present
NOAA-19	02/06/09	1400	0200	06/02/09 - present
MetOp A[3]	10/19/06	2130	0930	06/20/07 - present
MetOp B[3]	09/17/12	2130	0930	04/24/13 - present
Suomi NPP	10/28/2011	1330	0130	11/24/11 - present
NOAA-20	11/18/2017	1330	0130	11/29/17 - present
NOAA-21	11/10/2022	1330	0130	12/05/22 - present

[1]An ascending node would imply a northbound Equatorial crossing while a descending node would imply a southbound Equatorial crossing.
[2]Service date is according to Kidwell et al. (1995) and POES Status at Office of Satellite Operations, NESDIS. Information from the latter is used if there is any discrepancy between these two.
[3]Operated by European Space Agency (ESA) and is part of EUMETSAT's Polar System (EPS).

The AVHRR and VIIRS are the instruments that fly on all NOAA POES satellites including JPSS. The AVHRR instruments onboard TIROS-N, NOAA-6, NOAA-8, and NOAA-10 are designated as AVHRR/1, which has only four spectral channels. The AVHRR onboard NOAA-7, NOAA-9, NOAA-11, and NOAA-14 are designated as AVHRR/2, which operates in

five spectral channels. A version of the AVHRR with six spectral channels, AVHRR/3, is used on NOAA-15 and beyond. Channel 3a, with central wavelength at 1.61 μm, operates in the daylight part of the orbit while channel 3b operates in the night portion of the orbit. Channel 3a and channel 3b cannot operate simultaneously. The VIIRS instrument can collect data in 22 different spectral bands of the electromagnetic spectrum, in the wavelengths between 0.412 μm and 12.01 μm. The spatial resolution of the sensor depends on the band of the electromagnetic spectrum. Out of the 22 different spectral bands that the sensor has, 16 are moderate resolution bands (M-bands) , the other six bands are made up of five imaging resolution bands (I-bands), and one day/night panchromatic band with a spatial resolution of 750m. VIIRS imaging optics include a 19.1 cm Aperture and a 114 cm Focal length. Two I bands (I1 and I2) are selected to match AVHRR channel 1 and 2, and three M bands (M12, M15, and M16) are selected to match AVHRR channel 3b, Channel 4, and channel 5. The specifications of the AVHRR/VIIRS channels are listed in Table 3.

The AVHRR instrument scans in the cross-track direction with a field-of-view (FOV) of ±55.37° from nadir and has an instantaneous FOV (IFOV) of 1.1 km at nadir (1.3-1.4 milliradians by 1.3-1.4 milliradians for all channels). The full resolution AVHRR data are stored and processed in the High Resolution Picture Transmission (HRPT) and Local Area Coverage (LAC) outputs. The full resolution data is also processed onboard the satellite into Global Area Coverage (GAC). To produce GAC data, four out of every five samples along the scan line are used to compute one average value and the data from only every third scan line are processed. This yields a 1.1 km by 4 km resolution at the subpoint with a 3.3 km gap between pixels across the scan line at nadir. Generally, the GAC data are considered to have a 4 km resolution. Details of the AVHRR instruments and data can be found in Kidwell et al. (1995, 2009).

The VIIRS instrument scans in the cross-track direction with a field of view of ±56.28° degrees from nadir. This means that the VIIRS instrument can see a swath of land that is 112.37° wide as it scans across the Earth. The swath width of the VIIRS instrument is 3,060 kilometers, so at an altitude of 824 kilometers, the VIIRS instrument can see a strip of land that is about 1,901.4 miles (3,060 km) wide. The VIIRS instrument has a spatial resolution of 375 meters at nadir in the image-resolution bands (I-bands), and 750 meters in the M band. Similar to the AVHRR GAC data creation, VIIRS data is also processed to create VIIRS GAC data called VGAC data. The VGAC data is created by a team of scientists at NOAA's National Centers for Environmental Information (NCEI). The team first downloads VIIRS data from the NOAA CLASS website. The VIIRS data is then reformatted to match the ISCCP data format. The data is also reprojected to a common coordinate system.

Table 3: Spectral specifications of AVHRR/1, /2, /3, and VIIRS

CH	TIROS-N	NOAA-6,8,10	NOAA-7,9,11,12,14	NOAA-15 and onward	Suomi NPP, NOAA-20, and NOAA-21	GAC/VGAC nadir resolution (km)
	AVHRR/1	AVHRR/1	AVHRR/2	AVHRR/3	VIIRS	4.0
1	0.55-0.90 μm	0.58-0.68 μm	0.58-0.68 μm	0.58-0.68 μm	0.60-0.68 μm	4.0
2	0.725-1.10 μm	0.725-1.10 μm	0.725-1.10 μm	0.725-1.00 μm	0.85-0.88 μm	4.0
3A				1.58-1.64 μm		4.0
3B	3.55-3.93 μm	3.55-3.93 μm	3.55-3.93 μm	3.55-3.93 μm	3.61-3.79 μm	4.0
4	10.50-11.50 μm	10.50-11.50 μm	10.30-11.30 μm	10.30-11.30 μm	10.26-11.26 μm	4.0
5	Ch4 repeated	Ch4 repeated	11.50-12.50 μm	11.50-12.50 μm	11.06-12.96 μm	4.0

The AVHRR GAC and VIIRS VGAC data are used to generate the Polar Pathfinder FCDR. Significant variations in the equatorial crossing time (ECT) of a satellite will impact the accuracy in generating a consistent time series. There have been considerable drifts in the NOAA POES ECTs, as shown in Figure 1. The APP and VPP are composited at 0400 and 1400 local solar time (LST) for the Arctic, and 0200 and 1400 LST for the Antarctic. Only the NOAA satellites listed in Table 4 are used in the creation of APP and VPP, because these satellites carry AVHRR or VIIRS instruments with all five channels and the ECT of these satellites are relatively consistent. Five-channel AVHRRs are needed for most geophysical parameter retrieval, so the NOAA satellites before NOAA-7 and even-numbered satellites before NOAA-11 are not included. It should be noted that NOAA-16 has Channel 3A/3B switch, while NOAA-18 and NOAA-19 have only Channel 3B after August 5, 2005. The 5 AVHRR-like VIIRS channels have been selected from Suomi NPP, NOAA-20, and NOAA-21 satellites to match NOAA-19 AVHRR channels, and also calibrated to NOAA-19 5 AVHRR channels as described later in this document.

Table 4: NOAA POES satellites used in Polar Pathfinder FCDR.

NOAA satellite	Time range	Note
NOAA-7	01/01/82 – 12/31/84	
NOAA-9	01/01/85 – 11/07/88	
NOAA-11	11/08/88 – 12/31/94	
NOAA-14	01/01/95 – 12/31/00	
NOAA-16	01/01/01 – 08/09/05	NOAA-16 has Channel 3A/3B switching
NOAA-18	08/10/05 – 12/31/2014	On 08/05/05, automatic 3A/3B channel switching was disabled. Channel 3B is permanently on NOAA-18.
NOAA-19	1/1/2015-present	
Suomi NPP, NOAA-20, NOAA-21	1/5/2012-present	

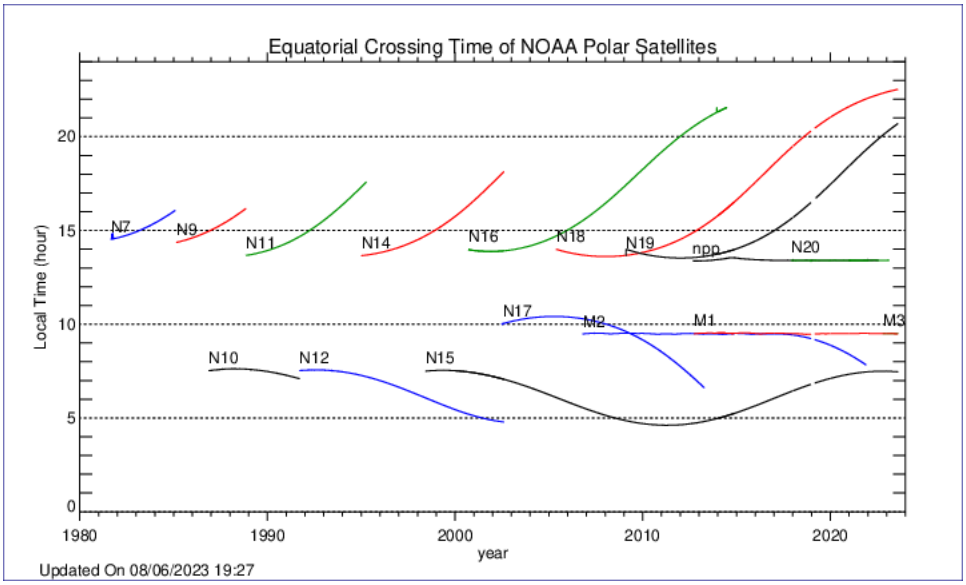

Figure 1: Equatorial crossing time of NOAA POES. (Figure is from www.star.nesdis.noaa.gov/smcd/emb/vci/VH/vh_avhrr_ect.php. The original ECT data are from www.ospo.noaa.gov/Products/ppp/navpage.html.)

3. Algorithm Description

3.1 Algorithm Overview

The generation of Polar Pathfinder FCDR daily composites includes the following steps:

1. AVHRR/VIIRS GAC/VGAC data from NOAA POES/JPSS from the previous day, current day, and the next day are acquired. Approximately 23 overpasses will potentially be used.
2. AVHRR/VIIRS GAC/VGAC data are calibrated following the steps in section 3.4.1 to obtain the visible channel reflectances and thermal channel Brightness Temperatures (BT).
3. AVHRR/VIIRS GAC/VGAC data are navigated following steps in section 3.2.3 to obtain accurate longitude/latitude and viewing angles.
4. Overpasses within a time window centered on 0400 and 1400 local solar time (LST) for the Arctic, and 0200 and 1400 LST for the Antarctic, are combined/composited based on sensor scanning angle and time difference from the target time.

The twice-daily composites that comprise the Polar Pathfinder FCDR consist of AVHRR/VIIRS channel reflectances and brightness temperatures, sensor scan angle, solar zenith angle, sun-sensor relative azimuth angle, Universal Coordinated Time (UTC) of the data acquisition, and a surface type mask.

3.2 Processing Outline

The four main steps used to generate the APP FCDR are outlined in Figure 2. Each step is explained in the following paragraphs.

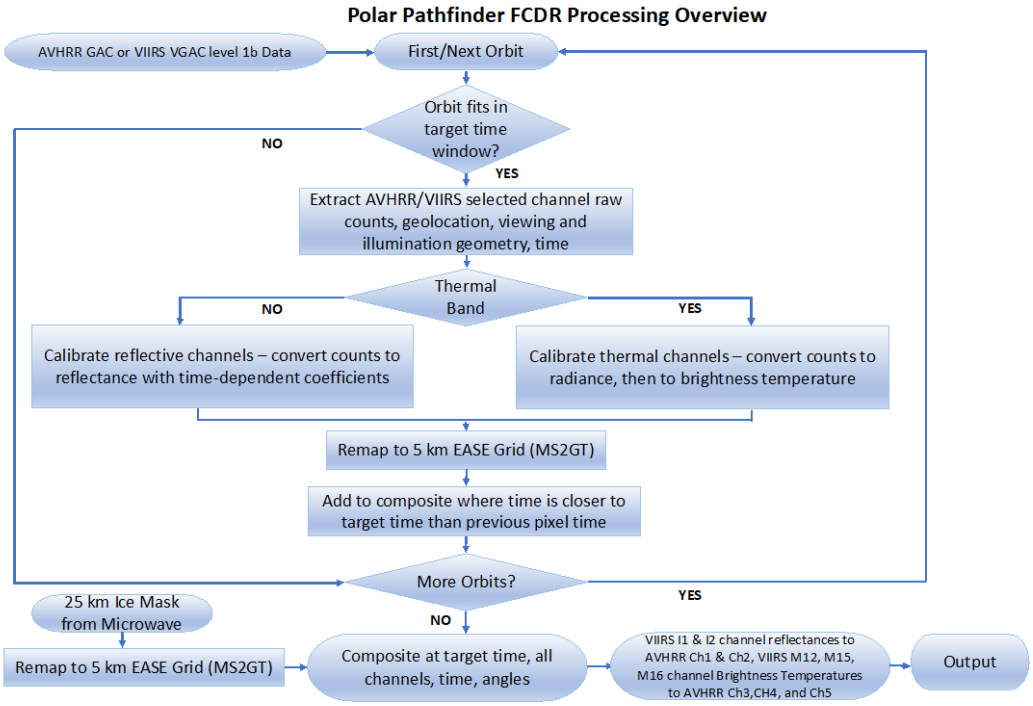

Figure 2: Flow chart of processing steps to generate Polar Pathfinder FCDR from AVHRR GAC and VIIRS VGAC level 1b data for a single target time.

3.2.1 Data Ingest

Step 1 is data ingest. For a daily composite, AVHRR/VIIRS GAC/VGAC data, at roughly 4 km spatial resolution, for all satellite overpasses with ending time after 12 UTC of the previous day, the current day, and starting time before 4 UTC of the next day are acquired. The approximate number of overpasses that go into each of the twice-daily composites is 23.

3.2.2 Calibration

Step 2 is calibration and inter-calibration. Calibration and inter-calibration are described in section 3.4.1, *Physical and Mathematical Description*.

3.2.3 Navigation

Step 3 is navigation. Each scan line in AVHRR/VIIRS GAC/VGAC data contains 409 viewed spots, but only 51 of those are geolocated in the level 1b data. The geolocations, longitude and latitude, of the 25th data sample and every 40th thereafter are included in the level 1b data by the Advanced Location Data System during the preprocessing of the data on the ground. A five-point Lagrangian interpolation is applied to derive the longitude/latitude for 2048 LAC pixels at 1.1 km resolution, from which the longitude/latitude of the 409

GAC/VGAC pixels are extracted. For regions north of 85 degrees north or south of 85 degrees south, the interpolation is done in the Gnomonic Space (Sullivan and Jelenak, 2007). The viewing angles are all interpolated using linear interpolation.

3.2.4 Compositing

Step 4 is compositing. In this step, all calibrated overpasses are composited. There are two daily composites in the 5 km EASE Grid for both the Arctic and the Antarctic with dimensions N by N, where N is 1805 for Arctic and 1605 for the Antarctic. For the Arctic, the two composites are for target times of 0400 and 1400 Local Solar Time (LST), respectively. For the Antarctic the two target times are 0200 and 1400 LST.

Data in each overpass from the first three steps are remapped to the 5 km EASE Grid based on longitude/latitude. The grid is then filled with data from the various overpasses in the following way. First, only those pixels in the overpasses whose time is within 3 hour of the target time are considered. Second, a pixel in an overpass updates the composite image pixel if the sensor scan angle for that pixel is less than (closer to nadir) the one that was previously used.

This method minimizes the scan angle dependence of the daily composite at the possible expense of obtaining an observation further from the target time. This is reasonable because retrievals of many geophysical parameters are strongly dependent upon scan angle, with uncertainty typically increasing at large scan angles.

Each composite time utilizes up to 23 overpasses, 14 from the current day, 7 from the day before, and 2 from the day after. It should be noted that the composites are for local solar time, not a fixed synoptic (UTC) time.

3.3 Algorithm Input

3.3.1 Primary Sensor Data

Every overpass of AVHRR GAC data from January 1, 1982 and VIIRS VGAC data from January 5, 2012 to the present for NOAA satellites listed in Table 4 is used to generate the APP and VPP. This data set can be ordered from the NOAA's Comprehensive Large Array-data Stewardship System (CLASS).

3.3.2 Ancillary Data

A surface mask is also included in the Polar Pathfinder FCDR output. It is not needed for, and is not part of, the AVHRR/VIIRS processing but rather is included as it may be of value in some user applications. For years prior to 1995, the surface mask is generated as follows. The daily averaged Polar Gridded Brightness Temperature of Special Sensor Microwave/Imagers (SSM/I) onboard the Nimbus-7 Scanning Multichannel Microwave Radiometer (SMMR) and the Defense Meteorological Satellite Program (DMSP) were regrided to the 25 km EASE Grid. Surface type, including land, ice sheets, and ocean are then identified. Over oceans, the NASA Team Sea Ice Algorithm was used to generate first-year and multi-year ice concentrations. In some cases, atmospheric effects and wind

roughening of the ocean cause false ice concentration retrievals over open ocean. Such areas will appear as incorrectly mapped areas of sea ice in the mask. Areas that consist of at least 50 percent multi-year ice are assigned the multiyear ice flag.

The multiyear ice estimate is subject to considerable error and uncertainty, particularly during periods when surface melt is likely (Cavalieri et al., 1999). At such times, characteristic multiyear ice emission properties are partially or completely hidden, and melt-freeze metamorphosis or other changes in the snow cover on sea ice may cause first-year ice to appear as a fraction of multi-year ice. Since thresholds were applied to the output from ice concentration, ice type, and snow depth algorithms, slight variations in the values yield a noisy appearance in the resulting binary flag images, particularly in spring and summer due to algorithm limitations. Over land, snow cover is detected with an SSM/I algorithm described in Goodison (1989). A gradient value (19 GHz horizontal polarization minus 37 GHz horizontal polarization) greater than zero indicates snow and the pixel is assigned a snow surface type. Special cases such as melting snow are not addressed in this mask. The SSM/I data have different coverage areas and thus the regriding process of the SSM/I leaves some areas without information over certain regions. The Near-Real-Time SSM/I EASE Grid Daily Global Ice Concentration and Snow Extent and Northern Hemisphere EASE Grid Weekly Snow Cover and Sea Ice Extent products from NSIDC were used to fill in the missing regions wherever possible. The resulting 5 km mask is over-sampled from the 25 km SSM/I data. Because coastal areas have a jagged appearance, a 5 km land mask is applied to the surface mask and the nearest appropriate surface type mask is used.

After the year 1995, the surface mask is from the Near-Real-Time SSM/I-SSMIS EASE Grid Daily Global Ice Concentration and Snow Extent, Version 4 (Nolin et al. 1998). This data set is in 25 km EASE Grid projection, which is then re-gridded to 5 km EASE Grid for APP.

3.3.3 Derived Data

There are no derived parameters in Polar Pathfinder FCDR beyond the calibrated and navigated reflectances and brightness temperatures. It is the primary input to the extended AVHRR/VIIRS Polar Pathfinder Product, APP-x/VPP-x. APP-x/VPP-x is described in a separate C-ATBD.

3.3.4 Forward Models

The Moderate resolution Imaging Spectroradiometer (MODIS) Swath-to-Grid Toolbox (MS2GT) is a set of software tools that reads HDF-EOS files containing swath data and produces flat binary files containing gridded data in a variety of map projections. MS2GT was originally written to map/grid MODIS data but it can be used with many types of satellite data. MS2GT consists of three Perl programs that make calls to several standalone IDL and C programs: mod02.pl which reads MOD021KM, MOD02HKM, or MOD02QKM Level 1b files, mod10_l2.pl which reads MOD10_L2 snow cover files, and mod29.pl which reads MOD29 sea ice files. All three Perl programs can optionally read MOD03 files for geolocation information. In addition, mod02.pl can extract ancillary data (such as illumination and viewing angles) from MOD03 files.

The MS2GT software is used to remap the calibrated AVHRR/VIIRS GAC/VGAC data at 4 km spatial resolution to 5 km EASE Grid. In this application, IDL programs are written to prepare the inputs to MS2GT, and process the outputs of MS2GT.

3.4 Theoretical Description

Polar Pathfinder FCDR has two daily composites derived from AVHRR/VIIRS GAC/VGAC data for both polar regions. The entire process consists of four main steps, extraction of the input data, calibration of the original data, navigation of each pixel of observations, and composition of all overpasses in three days as explained in details in section 3.2.

3.4.1 Physical and Mathematical Description

3.4.1.1 Reflectance Channel Calibration

The calculation of calibrated reflectance is fairly simple. The basic order of operations is this for data from each of the three channels:

1. Read in raw count, dark count, angles, sun-earth distance, time, and navigation from Level1b file.
2. Read in constants from the instrument file.
3. Compare dark count to average dark count. Reject the observation if different by more than 5 counts.
4. Subtract dark count from the raw count to get relative count or subtract the switch count (the count at which the gain switches) from the raw count to get high gain relative count.
5. Compute days since launch using time (1b) and launch date (instrument file).
6. Compute calibrated slope using days since launch and calibration parameters (instrument file).
7. Multiply relative count by calibrated slope to get calibrated reflectance.
8. Correct for sun-earth geometry using sun-earth distance and solar zenith angle.
9. Correct navigation.
10. Write reflectances and related variables (angles, time) to output file.

Reflectance is obtained from an electronic instrument in the following way: The instrument's sensors are sensitive to a certain band of wavelengths. The AVHRR/VIIRS

instrument has sensors that are capable of measuring energy in the visible (Channel 1/I1), the near infrared (Channel 2/I2), and the middle infrared (Channel 3a). The spectral response functions for these three AVHRR/VIIRS channels can be found at http://www.star.nesdis.noaa.gov/smcd/spb/calibration/avhrr/nrf.html and https://ncc.nesdis.noaa.gov/VIIRS/VIIRSSpectralResponseFunctions.php. The electronics convert the energy sensed in the band to a digital count. The greater the magnitude of this energy (signal), the larger the count. The older AVHRRs, AVHRR/1 and AVHRR/2, have a linear signal count response or gain, while the AVHRR/3s have a two-segment linear gain. The sensor also points into deep space during one part of each scan to record a dark count. The dark count is used to anchor the reflectance equation at zero. A calibration slope is used to convert the counts to reflectance units. This slope includes any factors involved: spectral response function, solar constant, instrument gain, etc.

$$R_u = S*(C - C_0)$$

Where R_u is the reflectance unadjusted for sun-earth distance or solar zenith angle, S is the calibration slope, C is the instrument count, and C_0 is the dark count. For AVHRR/3, counts below the switch count use the above equation with the low gain slope. For counts above the switch count, the switch count is used for C_0, and the high gain slope applied.
Some calibrations, such as those published in the polar orbiter data (POD) and NOAA KLM Guides, use a slope and intercept directly on the count and do not use the dark count. Using or not-using the dark count is built into any calibration, and is neither right nor wrong, as long as the calibration can return a zero reflectance for counts below some threshold.

The AVHRR/VIIRS calibration is originally done pre-launch, but once the instrument is launched, this calibration typically changes (immediately, due to launch conditions, and over time as the instrument ages). After launch, the instrument can only be calibrated indirectly, as there is no on-board calibration source for Channels 1, 2, and/or 3A. The computation of the calibration slopes, S, is described in section 3.4.4 and in Heidinger et al. (2010) and Molling et al. (2010). The ATBD for the AVHRR Channel 1 and 2 calibrations and VIIRS I1 and I2 calibrations are also available at https://www.ncei.noaa.gov/pub/data/sds/cdr/CDRs/AVHRR-HIRS_Reflectance_PATMOS-x/AlgorithmDescription%20_01B-1c.pdf and https://www.star.nesdis.noaa.gov/jpss/documents/ATBD/D0001-M01-S01-003_JPSS_ATBD_VIIRS-SDR_E.pdf, respectively.

3.4.1.2 Thermal Channel Calibration

The steps of calibration for the AVHRR thermal bands, channel 3b, channel 4 and channel 5, are mainly following the steps listed in chapter 7.1.2.4 in Kidwell et al. (2009). They are used for both AVHRR pre-KLM and KLM.

1. The temperature of the internal blackbody target is measured by four platinum resistance thermometers (PRT). On each scanline, a different PRT is sampled and three readings are recorded; on the fifth scanline all three PRT values for each PRT are set equal to 0 to indicate

that a set of four PRTs has just been sampled. The temperature of each PRT, T_{PRT}, is calculated based on C_{PRT} with coefficients d_1, d_2, d_3, d_4, where C_{PRT} is the mean of the three readings of each PRT.

$$T_{PRT} = d_0 + d_1 C_{PRT} + d_2 C_{PRT}^2 + d_3 C_{PRT}^3 + d_4 C_{PRT}^4$$

The coefficients d_0, d_1, d_2, d_3, d_4, are available from tables in Appendix D in Kidwell et al (2009) and also included in the ancillary files of this algorithm. The internal blackbody temperature T_{BB} is then derived with consideration of T_{BB} values from previous calculations.

$$T_{BB} = (1 - SW) T_{BB1} + SW * T_{BB2}$$

T_{BB1} is the blackbody temperature of the previous scan line, and T_{BB2} is the blackbody temperature of the current scan line. SW is the smoothing weight set at 0.2.

2. The radiance N_{BB} sensed in each thermal AVHRR channel for the internal blackbody at temperature T_{BB} is calculated with a rapid Planck calculation using a lookup table approach. Cold space radiance N_s is a constant for each satellite, and is read in from ancillary files.

3. Mean count values of the 10 AVHRR views of the internal blackbody and cold space targets, C_{BB} and C_S are calculated with consideration of values from previous calculations with a smoothing weight of 0.2. The linear slope C_E and intercept *I* to convert the count output of AVHRR viewing the Earth targets to linear radiance estimate N_{LIN} is

$$N_{LIN} = M * C_E + I$$

where $M = (N_S - N_{BB}) / (C_S - C_{BB})$, and $I = Ns - M * C_S$.

Nonlinear response of radiance is added to N_{LIN} to get the final radiance N_E,

$$N_E = N_{LIN} + N_{COR}$$

The nonlinear correction of radiance is based on the linear radiance as

$$N_{COR} = b_0 + b_1 N_{LIN} + b_2 N_{LIN}^2$$

where b_1, b_2, and b_3 are coefficients based on post-launch research work (Kidwell et al. 2009), and are read from the ancillary files. All the coefficients are included in the instrument constant files discussed in section 3.3.2.

The corrected radiance is then converted to brightness temperatures with a rapid Planck calculation using a lookup table approach.

The ATBDs for the AVHRR and VIIRS thermal channel calibrations are also available at https://www1.ncdc.noaa.gov/pub/data/sds/cdr/CDRs/AVHRR_Radiances_NASA/AlgorithmDescription_01B-30a.pdf and https://www.star.nesdis.noaa.gov/jpss/documents/ATBD/D0001-M01-S01-003_JPSS_ATBD_VIIRS-SDR_E.pdf, respectively.

3.4.1.3 Calibration of VIIRS channels to AVHRR Channels

For the consistence with current AVHRR 5 channels in APP CDR and the current algorithms used in the following APP-x CDR process for the purpose of extending current APP/APP-x CDRs to the VIIRS era, VIIRS 5 channels that are closest to AVHRR 5 channels in spectrum were selected to be used for generating VPP and VPP-x CDRs that are cconsistent and matched with APP/APP-x CDRs in variable and in time. The selected 5 VIIRS channels are I1, I2, M12, M15, and M16 corresponding to AVHRR Channel 1, channel 2, channel 3b, channel 4, and channel 5.

For the purpose of applying current algorithms used with AVHRR channels, VIIRS channels need to be calibrated in terms of NOAA-19 AVHRR channels. A multivariable regression approach was adopted to find a method to do inter-calibration between AVHRR and VIIRS by using the data from both AVHRR and VIIRS that are matched each other in time and in place. The equation used to calibrate VIIRS channel reflectance and brightness temperature to NOAA-19 AVHRR reflectance and brightness temperature is as

$$C_{av} = a_0 + a_1 * C_{vi} + a_2 * A_{sc} + a_3 * A_{sz} + a_4 * A_{ra}$$

where C_{vi} is VIIRS channel reflectance (I1 or I2) or brightness temperature (M12, M15, or M16), C_{av} is NOAA-19 AVHRR channel reflectance (channel 1 or 2) or brightness temperature (channel 3b, 4, or 5) corresponding to VIIRS channels after calibration, A_{sc} is VIIRS scan angle, A_{sz} is VIIRS solar zenith angle, A_{ra} is VIIRS relative azimuth angle, a_0, a_1, a_2, a_3, and a_4 are the regression coefficients dependent upon the channel selection, hemisphere selection, and time selection. Those regression coefficients are listed in the Appendix B.

3.4.2 Data Merging Strategy

Data merging, i.e., compositing, is described in section 3.2.4.

3.4.3 Numerical Strategy

Not Applicable.

3.4.4 Calculations

Once the channel counts are read in, the space count or switch count is subtracted to form a relative count, C_{rel}, and then the calibration is applied. The calibration converts raw counts to reflectance. The calibration parameters are a function of time since launch:

$$S(t) = S_0 (100 + S_1 t + S_2 t^2)/100$$

where S is the calibration slope (reflectance in %/count), S_0 , S_1, and S_2 are the calibration terms, and t is the time in years since launch. If the instrument is dual gain, the raw absolute count is compared to the gain switch. If the count is less than the switch, the low gain calibration parameters are applied; if above, the high gain calibration is applied. The calibration parameters S_0, S_1, and S_2, respectively, are in Table 5. S_0 is considered to be the calibrated slope at launch, while S_1 and S_2 are the time-dependent degradation coefficients.

These coefficients have been updated periodically after the paper published in 2010, and the latest coefficients are included in the ancillary files in this algorithm package.

Table 5: Calibration slope parameters for AVHRR channels 1 and 2 (Heidinger et al., 2010).

	Channel 1			Channel 2		
Satellite	S_0	S_1	S_2	S_0	S_1	S_2
TIROS-N	0.105	27.015	−12.876	0.121	10.709	−0.643
NOAA-6	0.088	47.977	−16.122	0.077	97.301	−32.590
NOAA-7	0.117	3.635	0.045	0.119	6.579	−0.620
NOAA-8	0.116	14.177	−2.729	0.132	12.611	−2.713
NOAA-9	0.110	3.242	0.793	0.117	2.365	0.155
NOAA-10	0.108	9.819	−1.615	0.127	5.201	−0.707
NOAA-11	0.114	0.022	0.091	0.116	0.299	0.045
NOAA-12	0.123	2.624	−0.116	0.147	1.191	−0.041
NOAA-14	0.120	5.034	−0.489	0.147	0.023	0.311
NOAA-15	0.121	0.447	−0.060	0.135	0.035	0.007
NOAA-16	0.112	0.306	0.025	0.116	0.586	0.036
NOAA-17	0.115	1.707	−0.151	0.130	3.117	−0.265
NOAA-18	0.111	3.068	−0.443	0.119	4.541	−0.611
NOAA-19	0.112	−5.985	−8.687	0.117	2.263	0.748
Metop-A	0.111	1.797	−0.352	0.127	2.149	−0.225

3.4.5 Look-Up Table Description

Other than the instrument files, discussed in Section 3.3.2, the only look-up tables used are clock correction tables stored in the code. These were obtained from the University of Miami (see http://yyy.rsmas.miami.edu/groups/rrsl/pathfinder/Processing/proc_index.html). These are used to correct navigation only. They do not alter reflectance values.

3.4.6 Parameterization

Not Applicable.

3.4.7 Algorithm Output

This algorithm generates the APP and VPP composites at 5 km EASE Grid twice daily over both poles, Arctic and Antarctic, from 1982 to the present. The twice daily composite consists of five AVHRR and VIIRS channel data, sensor scanning angle, solar zenith angle, sun-sensor relative azimuth angle. Complimentary data include the Universal Coordinated Time (UTC) of the data acquisition, and surface type mask. The daily Polar Pathfinder FCDR composites are centered on local solar times of 1400 (high sun, but could be nighttime for some polar areas in winter) and 0400 for the Arctic or 0200 for the Antarctic. Polar Pathfinder FCDR covers the Arctic from 48.4° N to the North Pole, and the Antarctic from -53.2° S to the South Pole. All the daily data at each LST for each pole are stored in one netCDF file, so there are four files for each year. The output details are listed in Table 6.

Table 6: Polar Pathfinder FCDR output

Name	File format and size	Content	Note
APP/VPP_n005_####_0400.nc APP/VPP_n005_####_1400.nc APP/VPP_s005_####_0200.nc APP/VPP_s005_####_1400.cn ####: year, e.g. 2000	netCDF, 22 gb (6gb) 22 gb (6gb) 17 gb (4gb) 17 gb (4gb) uncompressed (compressed)	Longitude Latitude Julian day Ch1 reflectance Ch2 reflectance Ch3 BT/reflectance Ch4 BT Ch5 BT Sensor scanning angle Solar zenith angle Sun-sensor relative azimuth angle UTC of observation	Degree, -180 to 180 Degree, positive for NH % % K/% K K Degree Degree Degree hhmmss

4. Test Datasets and Outputs

4.1 Test Input Datasets

For the Arctic composite, July 1 data for every year from 1982 to 2013 are used as the test datasets, both visible channel reflectance and thermal channel BT. For the Antarctic composite, January 1 data of every year from 1982 to 2013 are used. There is a total of 32 days of data available for both poles. The input data is the AVHRR GAC level 1b data from the University of Wisconsin Space Science and Engineering Center (SSEC) Data Center; they are identical to those data archived at NOAA CLASS. Daily APP composites are generated using these test input datasets.

4.2 Test Output Analysis

4.2.1 Reproducibility

Pixel-to-pixel comparisons of each of the APP output variables to those produced in test cases during the algorithm development process are performed to verify the output. Two examples of the output are shown in Figures 3 and 4. No discrepancies were found.

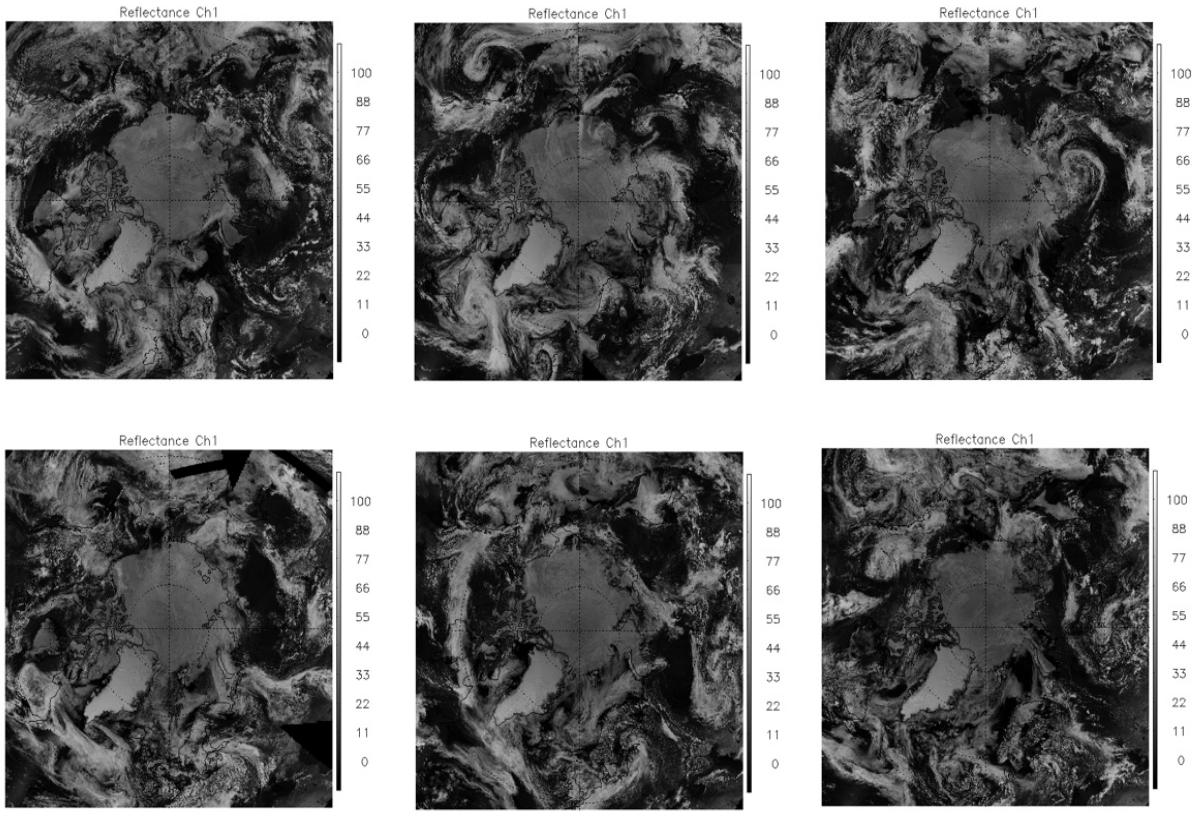

Figure 3: AVHRR channel 1 reflectance (%) at 1400 LST of the Arctic on July 1 of the year 1982, 1986, 1989, 1996, 2002, and 2007.

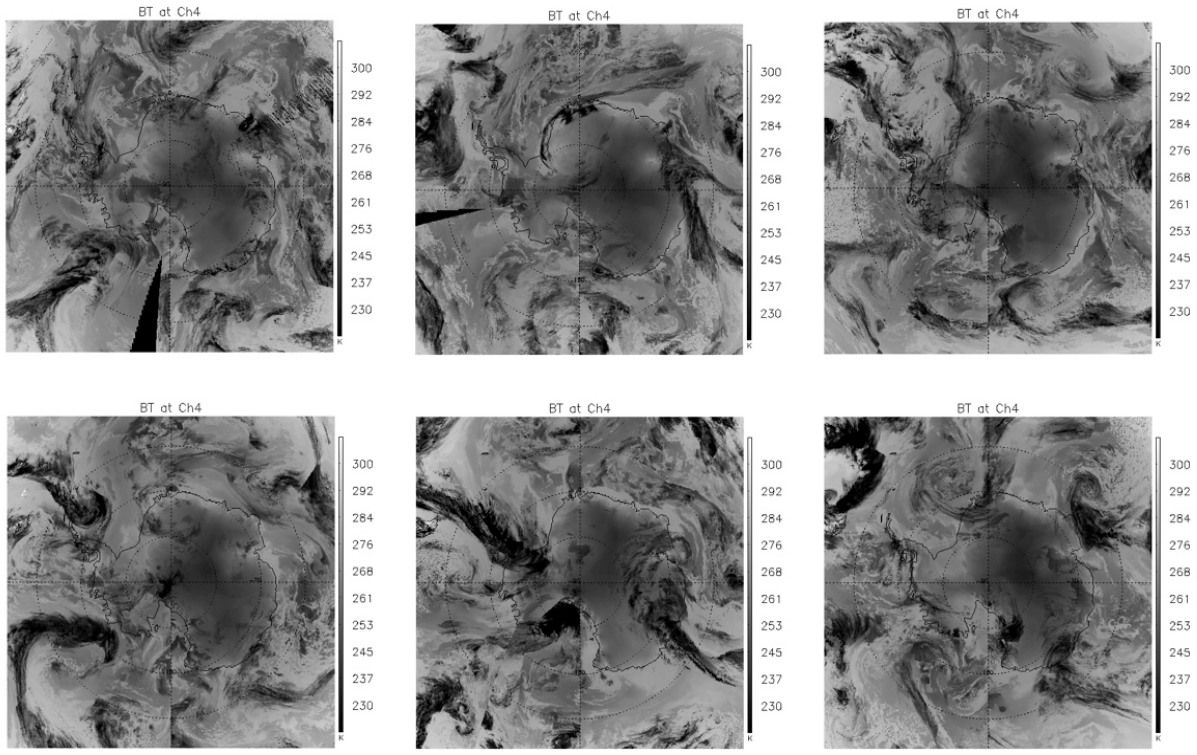

Figure 4: AVHRR channel 4 BT (K) at 1400 LST of the Antarctic on January 1 of the year 1982, 1986, 1989, 1996, 2002, and 2007.

4.2.2 Precision and Accuracy

Precision of reflectance starts with the fact that the input counts are 10bit. The full range in reflectance, 0 to about 110% (reflectances greater than 100% are possible) is represented by counts ranging from 0 to 1023, implying that the counts themselves allow a precision of about 0.1% in reflectance units. However, the calibration slope for each AVHRR determines the precision for that particular instrument and range. Channel 1 slopes at launch (and therefore precision values) range from 0.09 to 0.12 for single gain AVHRRs (TIROS-N through NOAA-14). Dual-gain AVHRRs have a higher precision in the low reflectance gain region and lower precision in the high gain region. This ranges (in reflectance units of %) for Channel 1, low gain, from 0.05 to 0.06, and high gain 0.17 to 0.20. Channel 2 precision at launch ranges from 0.08-0.13 for single gain, and 0.05-0.06 and 0.17-0.20 for low and high gain, respectively. Channel 3a is only present on dual gain AVHRRs, and precision at launch ranges from 0.02-0.03 for low gain and 0.18-0.22 for high gain. Slopes and precision values tend to increase after launch. The maximum slopes/precision values are 0.14 for Ch1, 0.22 for Ch2, and 0.24 for Ch3a.

Accuracy, on the other hand is determined by both the calibration and the method of producing the Level2b data. The accuracy of the calibration procedure with respect to MODIS Collection 5 is 2% for Channel 1 and 3% for Channel 2. Channel 3a's accuracy is 3%.

These accuracies are for the reflectance value itself. Thermal channel calibration errors are typically in the range 0.03 – 0.3K at 300K, depending on the channel and radiometer. The noise increases as temperature decreases (Trishchenko et al., 2002).

Level1b data contain navigation errors from 2 to 10 km (Heidinger et al. 2002). These errors introduce uncertainty in the actual location of each reflectance value of up to 20km. Improved orbit stabilization of the satellites bearing AVHRR/3s will contribute to higher accuracy reflectances due to higher accuracy navigation.

Additional comparisons to MODIS were done by generating a MODIS composite dataset similar in form to APP. Daily MODIS composites were generated at 0400 and 1400 LST at 5 km EASE Grid resolution using 1 km resolution MODIS Aqua data at similar channels as AVHRR channels, including MODIS channel 1 (0.62-0.67 μm), channel 2 (0.841-0.876 μm), channel 22 (3.929-3.989 μm), channel 31 (10.78-11.28 μm), and channel 32 (11.77-12.27 μm). A comparison of APP and MODIS Aqua composites provides a rough estimate of the precision and accuracy of APP composites. Figure 5 provides one example of such a comparison. For this case, the bias and standard deviation between APP and MODIS Aqua composites at 1400 LST of Arctic are -3.31% and 10.18% for channel 1, and 0.92 K and 8.21 K for channel 4. Other cases yield similar statistics. It should be noted that these two composites are at somewhat different wavelengths, times, and viewing angles. Differences of this magnitude are therefore reasonable.

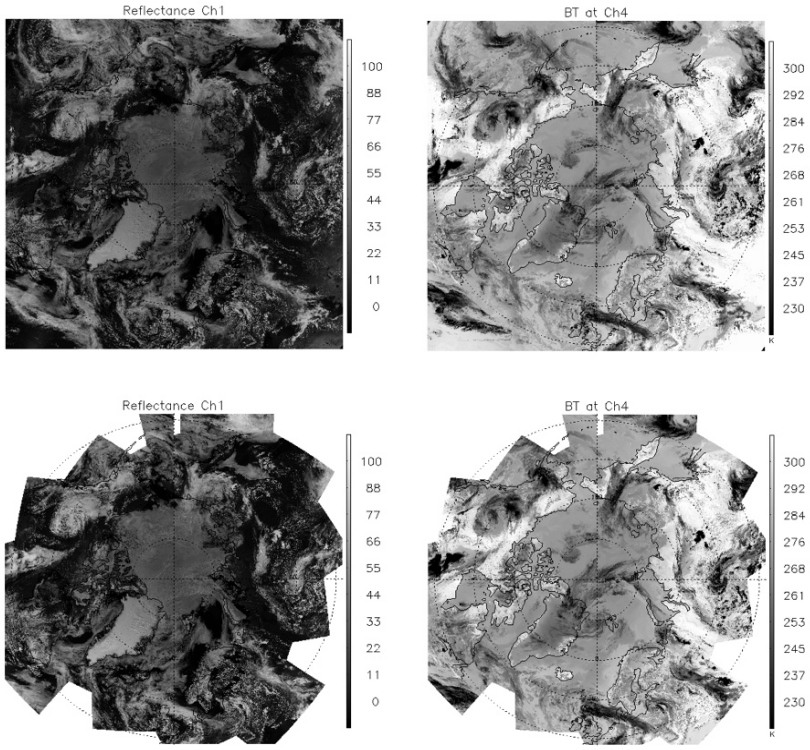

Figure 5: Channel 1 reflectance (%) and channel 4 BT (K) at 1400 LST of the Arctic on July 1 of the year 2007 from AVHRR (upper row) and MODIS Aqua (lower row).

4.2.3 Error Budget

Table 7 contains a summary of the known errors in calibration and navigation of AVHRR GAC data. See Section 4.2.2 for additional details and references.

Table 7: Summary of Errors in AVHRR Ch1, Ch2, and Ch3a reflectance data set.

Error	Magnitude of Error
Reflectance channel calibration errors	Ch1: 2%, Ch2: 3%, Ch3a: 3%
Thermal channel calibration error	0.03 – 0.3K at 300K
Level1b navigation error	Up to 20 km

4.2.4 Calibration of VIIRS Channels to NOAA-19 AVHRR Channels

As stated in the section 3.4.1.3, the selected VIIRS channel reflectance and brightness temperature are calibrated to corresponding NOAA-19 AVHRR reflectance and brightness temperature to make them as close as possible in value to allow next step APP-x data products processing by using the same algorithms to extend the current APP/APP-x CDRs to VIIRS era to create long-term, continuous, consistent, and valuable Climate Data Records (CDRs) across AVHRR and VIIRS eras.

The overlapped data over 2012-2016 from AVHRR and VIIRS were used in multi-variable regression approach for both poles, and the overlapped data over 2017-2019 from AVHRR and VIIRS were used as independent dataset to exam and verify the regression equation presented in the section 3.4.1.3. We selected the overlapped AVHRR and VIIRS data based on their locations, dates and time, scan angles, solar zenith angles, and relative azimuth angles. If those three angles differences between AVHRR and VIIRS are all in the range of +0.1 to -0.1 degrees, then the data from AVHRR and VIIRS are deemed overlapped for those pixels and dates, and used in the multi-variable regression for finding inter-calibration equation. Figure 6 provides one example of NOAA-19 AVHRR channel 1 and 2 reflectances (upper row) versus VIIRS band I 1 and I 2 reflectances (lower row) after inter-calibration on July 12 ,2017 at 14:00 local solar time for the Arctic region. For this case, the overall biases between APP and VPP composites at 1400 LST of Arctic are -0.91% and -0.16% for channel 1 and channel 2, respectively. Other cases yield similar statistics. It should be noted that these two composites are at somewhat different wavelengths, times, and viewing angles even after inter-calibration. Differences of this magnitude are therefore reasonable.

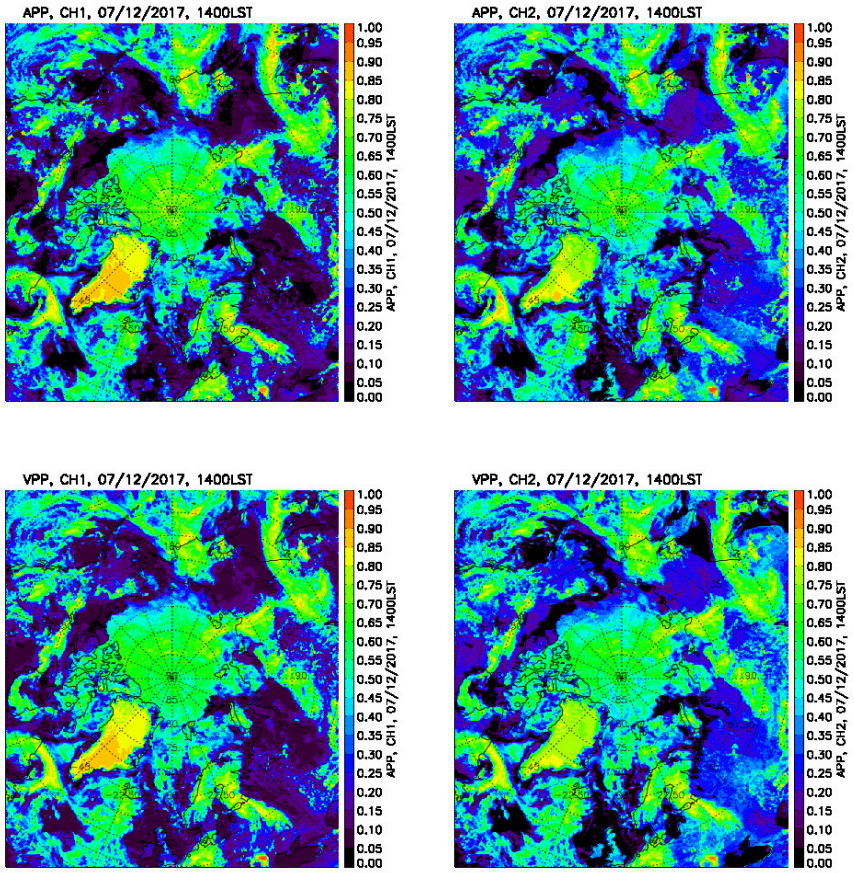

Figure 6: Channel 1 and channel 2 reflectances (%) at 14:00 LST of the Arctic on July 12, 2017 from AVHRR (upper row) and VIIRS (lower row).

Figure 7 provides another example of NOAA-19 AVHRR channel 3, 4, and 5 brightness temperature (upper row) versus VIIRS band M 12, M 15, and M 16 brightness temperature (lower row) after inter-calibration on July 12 ,2017 at 14:00 local solar time for the Arctic region. For this case, the overall biases between APP and VPP composites at 1400 LST of the Arctic are -1.19 K, and -0.15 K, and -0.45 K for channel 3, 4, and 5, respectively. As said above, It should be noted that these two composites are at somewhat different wavelengths, times, and viewing angles even after inter-calibration. Differences of these magnitudes are therefore reasonable.

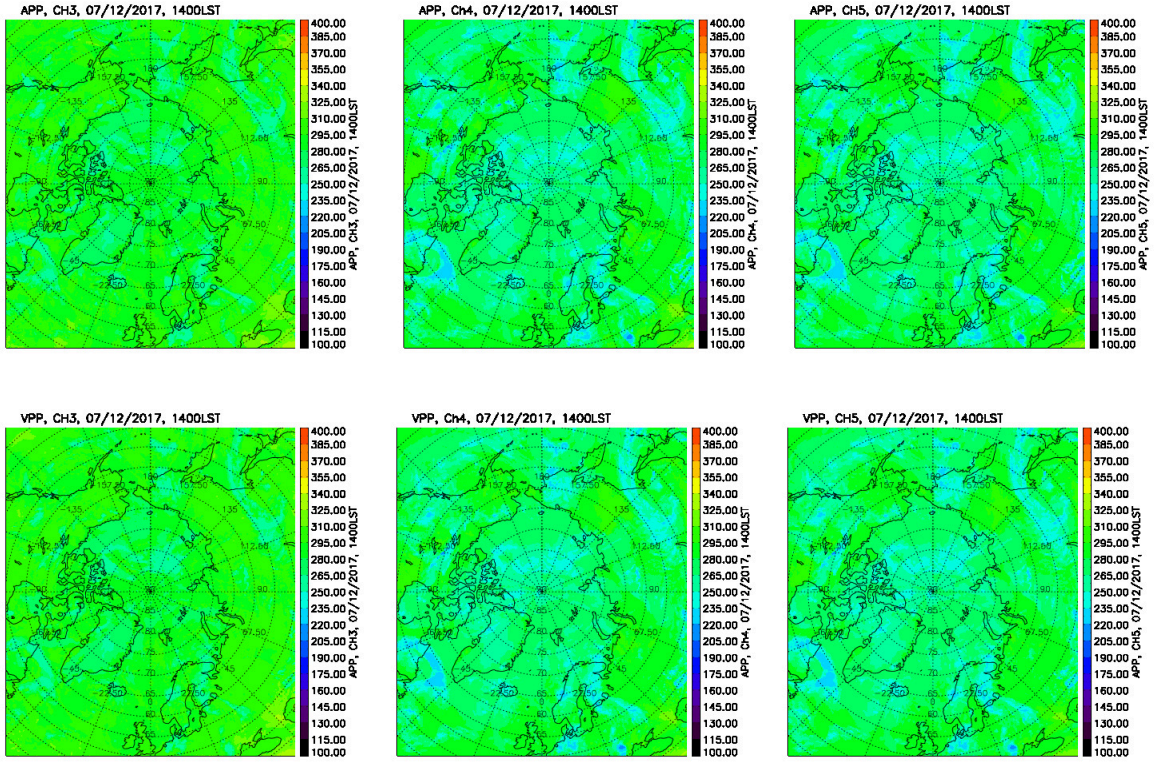

Figure 7: Channel 3, 4, and 5 brightness temperature (K) at 14:00 LST of the Arctic on July 12, 2017 from AVHRR (upper row) and VIIRS (lower row).

For climate study, a long-term Climate Data Record (CDR) should be carefully examed to guarantee that the data products ingested from different satellites are consistent in value over a long period of time. The time series of APP and VPP data products were compared to each other when and where they were overlapped to make sure that the data products in the CDR can be used for climate study within enough accuracy. Figure 8 provides some examples of the times series of NOAA-19 AVHRR channel 1 and 2 reflectances, channel 3, 4, and 5 brightness temperatures versus those of VIIRS band I 1 and I 2 reflectances, M 12, M 15, and M 16 brightness temperatures after inter-calibration over the year of 2017 at 14:00 local solar time for the Arctic region north of 60 degrees. For this case, the biases between APP and VPP composites are -0.91%, -1.15%, -0.88 K, 0.32 K, and 0.29 K, respectively. As said above, It should be noted that these two composites are at somewhat different wavelengths, times, and viewing angles even after inter-calibration. Differences of this magnitude are therefore reasonable.

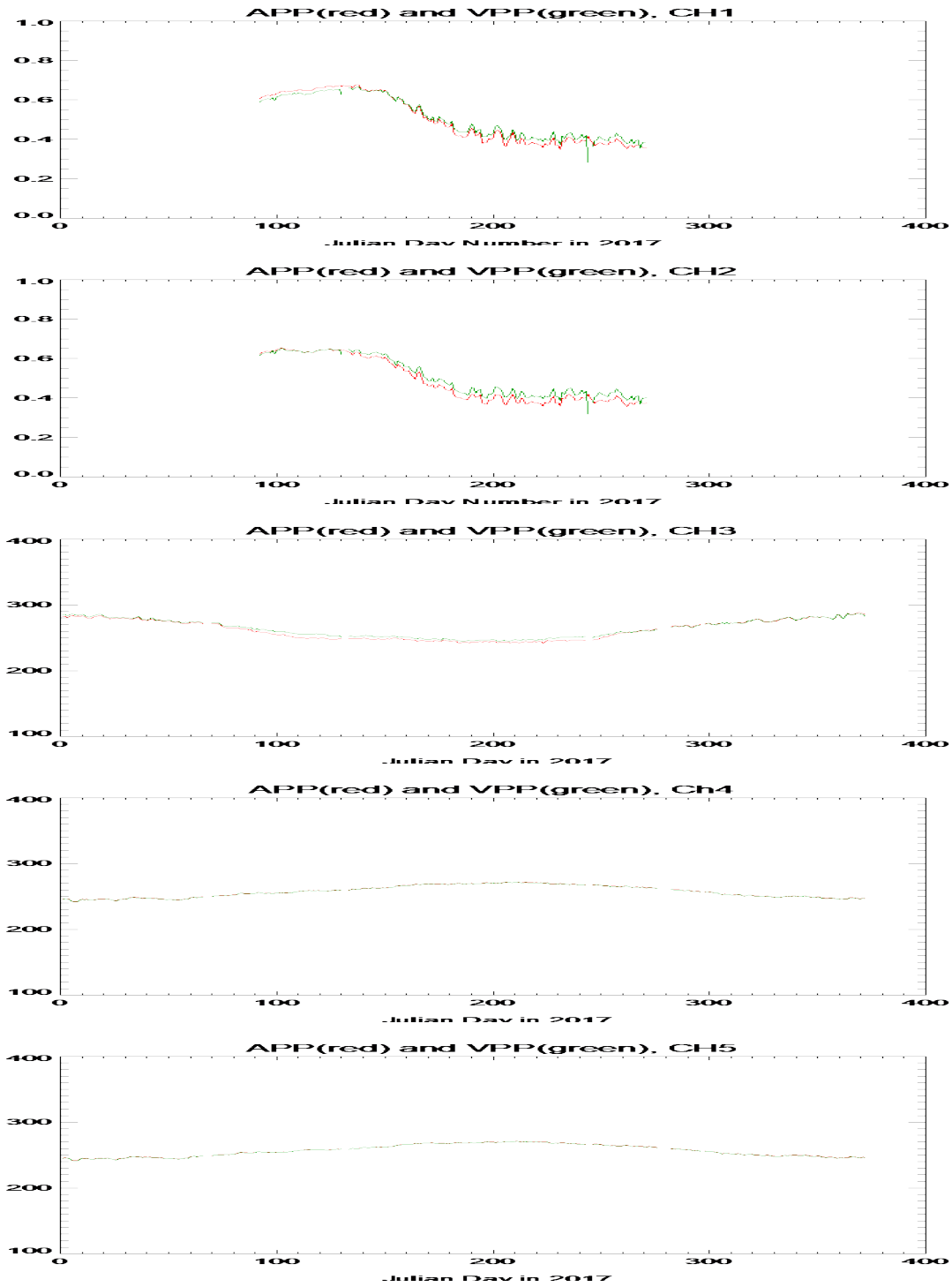

Figure 8: Times series of NOAA-19 AVHRR channel 1 and 2 reflectances, channel 3, 4, and 5 brightness temperatures (red) vs time series of VIIRS band I 1 and I 2 reflectances, M 12, M 15, and M 16 brightness temperatures (green) after inter-calibration over one year of 2017 at 14:00 LST for the Arctic region north of 60 degrees.

5. Practical Considerations

5.1 Numerical Computation Considerations

Not Applicable.

5.2 Programming and Procedural Considerations

On a Linux machine, running on a single 2.6 GHz Opteron™ Processor 4180, it takes 16 minutes to generate daily composites at two times per day for both poles. Prior to 2005, the codes are in Bash shell scripts and C programs.

5.3 Quality Assessment and Diagnostics

Current quality assessment is limited to out-of-range value detection and the number of missing (unfilled) pixels in the grid. Additional quality assessment and diagnostic statistics are being considered for future versions of the data.

5.4 Exception Handling

Error messages are recorded for every step of the processing.

5.5 Algorithm Validation

The calibration methods are provided by NOAA and have been validated by NOAA. Composite images have been “spot checked” manually against calibrated swath data and no discrepancies have been found.

5.6 Processing Environment and Resources

Before the year 2005, shell script and C programs are used to process the data on an x86_64 m64 server running the red hat Linux or CentOS operating system. After the year 2005, b shell script and IDL version 8.0 are used to process the data on an x86_64 server running the red hat Linux or CentOS operating system. The input for daily composite is around 2.4 GB, and output for annual data is 78 GB without compression.

6. Assumptions and Limitations

Not Applicable

6.1 Algorithm Performance

The performance of the calibration method has been documented elsewhere (Heidinger et al., 2010; Molling et al., 2010). On the inter-satellite differences are addressed here. We

have examined the time series of AVHRR brightness temperatures and reflectances for NOAA-7, -9, -11, and -14 over the period of 1982-1999. If the calibration procedures are effective, and if the changes in viewing/illumination geometry are small, there should be no obvious discontinuities across satellite boundaries. We use Barrow, Alaska as a "calibration" location because surface temperature measurements show no significant trend over the study period. Figure 9 shows the time series of channel 4 brightness temperatures for 1982-1999, a period covering four satellites (NOAA-7, -9, -11, and -14). The monthly average brightness temperatures were generated for a 275 x 275 km^2 area around Barrow at a local solar time of about 1400 LST. There is no obvious change from one satellite to the next that could be attributed to differences in calibration. (Note: From NOAA-11 to NOAA-14 there are no data available from September 14, 1994 to January 18, 1995.)

Figures 10 and 11 show the time series of AVHRR channel 4 brightness temperatures based on daily observations at Barrow. They clearly indicate that the change in satellites caused only a very small change of the brightness temperature, significantly less than the daily variation. The APP-x data set exhibits very good infrared channel intercalibration between NOAA-7, -9, -11, and -14. Figure 12 shows a time series of monthly average surface skin temperatures from the APP-x data set. The retrieval algorithm adjusts for viewing angle, so that orbital drift is even less of an issue than with brightness temperatures alone. There is no obvious discontinuity from one satellite to the next.

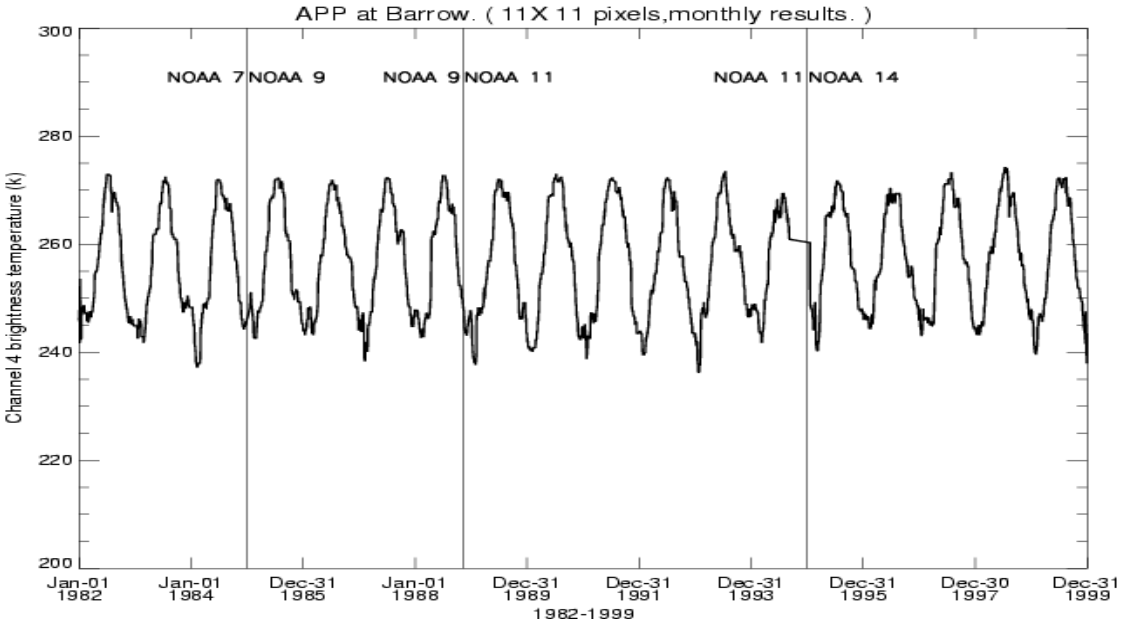

Figure 9: Time series of monthly average AVHRR channel 4 brightness temperatures from January 1, 1982 to December 31, 1999 at Barrow, Alaska for 1400 local solar time. Note: there are no data available from September 14, 1994 to January 18, 1995.

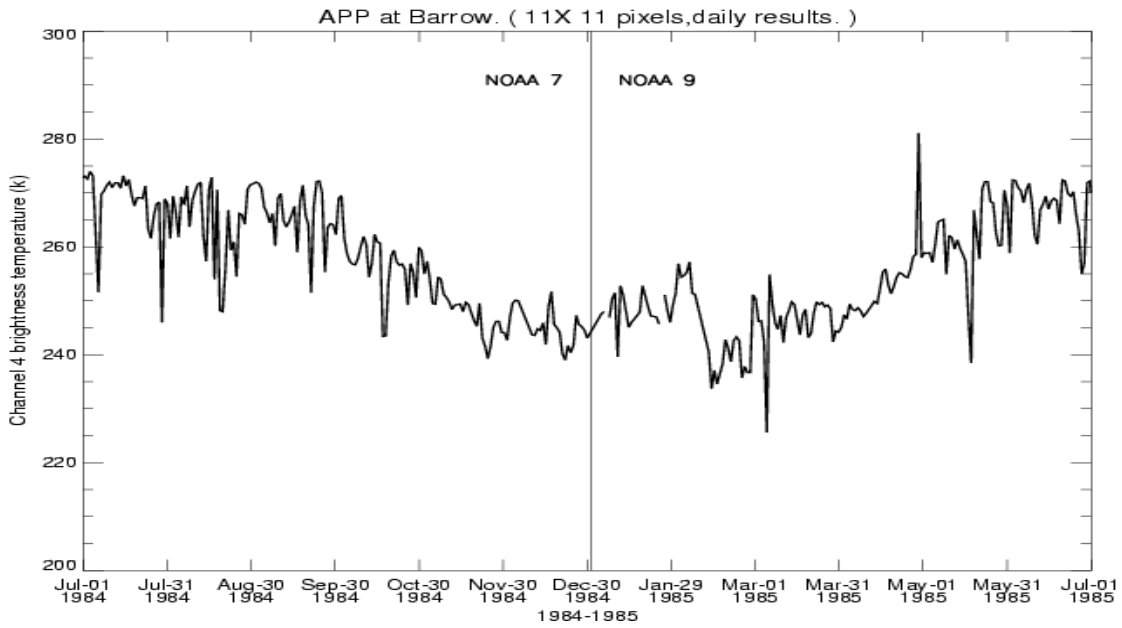

Figure 10: Time series of daily AVHRR channel 4 brightness temperatures from July 1, 1984 to July 1, 1985 at Barrow, Alaska for 1400 local solar time covering the change from NOAA-7 to NOAA-9 (vertical line).

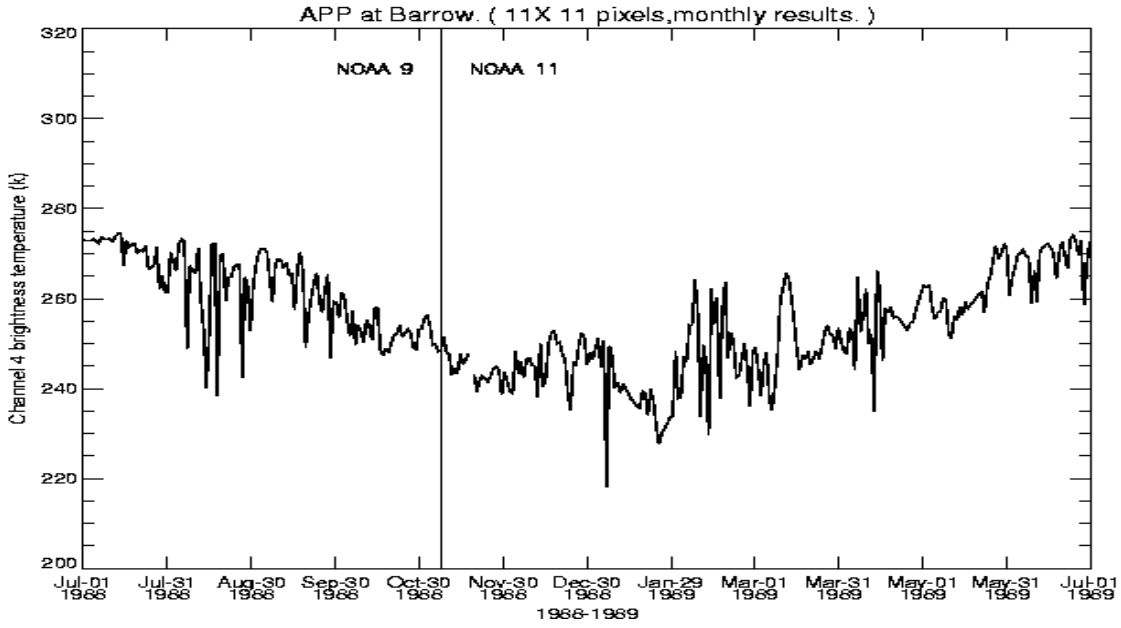

Figure 11: Time series of daily AVHRR channel 4 brightness temperatures from July 1, 1988 to July 1, 1989 at Barrow, Alaska for 1400 local solar time, covering the change from NOAA-9 to NOAA-11 (vertical line).

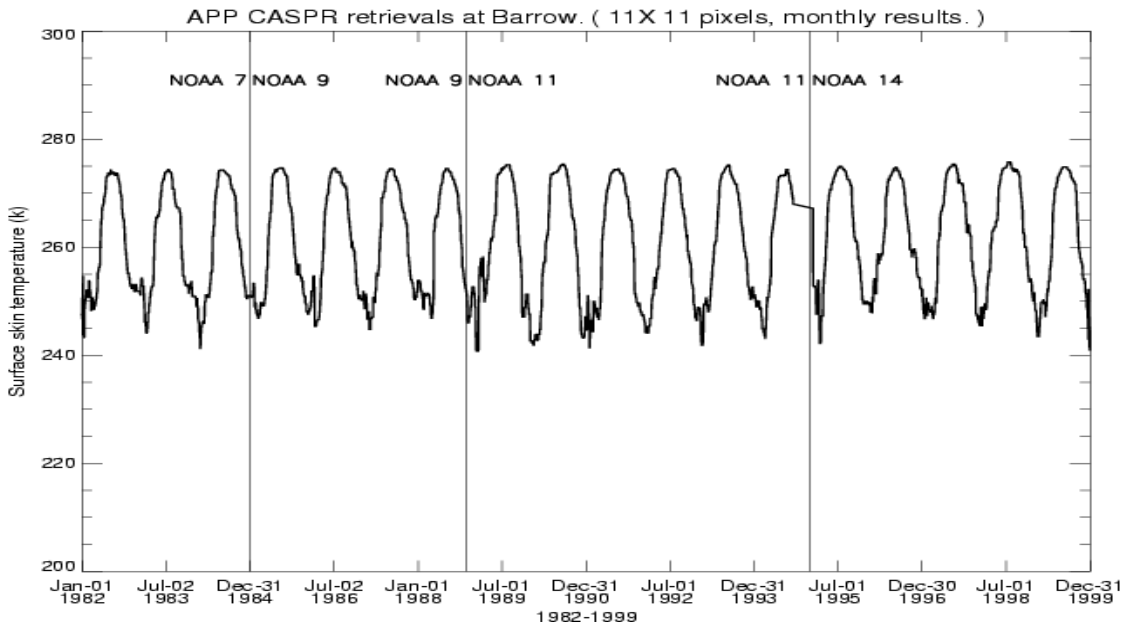

Figure 12: Time series of monthly average surface skin temperatures from January 1, 1982 to December 31, 1999 at Barrow, Alaska for 1400 local solar time. Note: there are no data available from September 14, 1994 to January 18, 1995.

Because the NOAA satellite transitions occurred during the Northern hemisphere winter, Vostok, Antarctica was used to examine the AVHRR visible channels. Due to orbital drift and different equator crossing times, significant changes in visible channel reflectances can be expected from one satellite to the next. Figure 13 shows the time series of the AVHRR channel 2 reflectances from July 1, 1984 to July 1, 1985 at 1400 local solar time over a 275 x 275 km^2 area around Vostok. There is a rather abrupt change at the time of the satellite transition.

Figures 14 and 15 show the time series of the sensor scan angles and solar zenith angles from July 1, 1984 to July 1, 1985 during the transition from NOAA-7 to NOAA-9. It shows that the solar zenith angle difference is small, but that the scan angles and relative azimuth angles changed significantly. The illumination and viewing geometry changes affect the AVHRR visible channel reflectances because of the anisotropic reflection and asymmetrical scattering characteristics of snow and clouds, which must be taken into account for surface albedo retrieval.

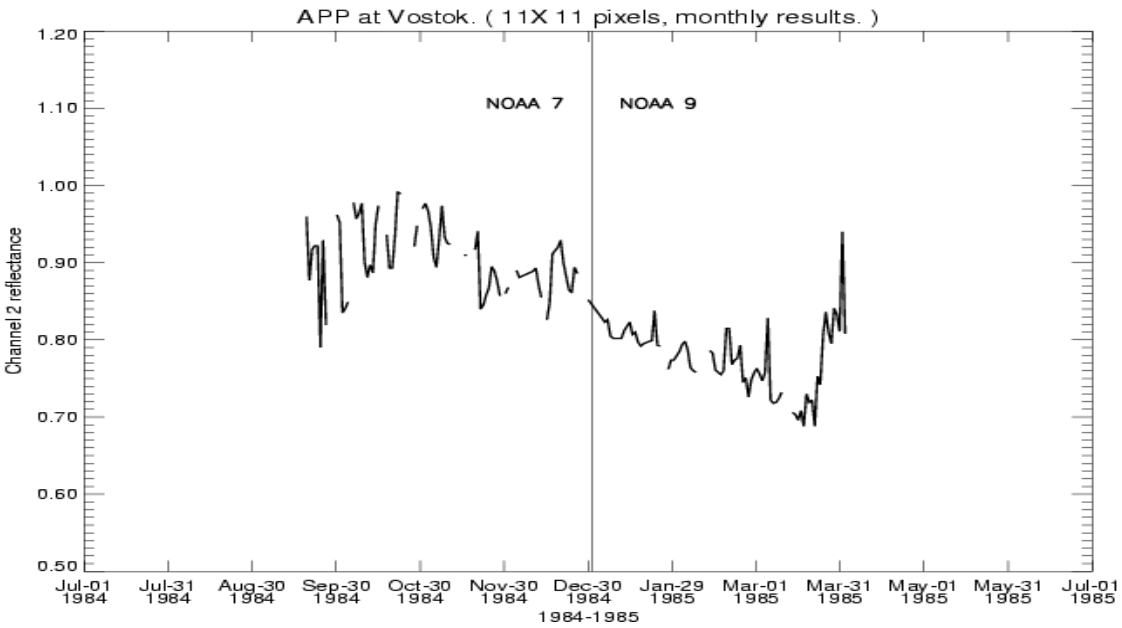

Figure 13: Time series of the AVHRR channel 2 reflectance averaged over a 275 x 275 km^2 area around Vostok, Antarctica from July 1, 1984 to July 1, 1985 at a local solar time of 1400, covering the transition of NOAA-7 to NOAA-9.

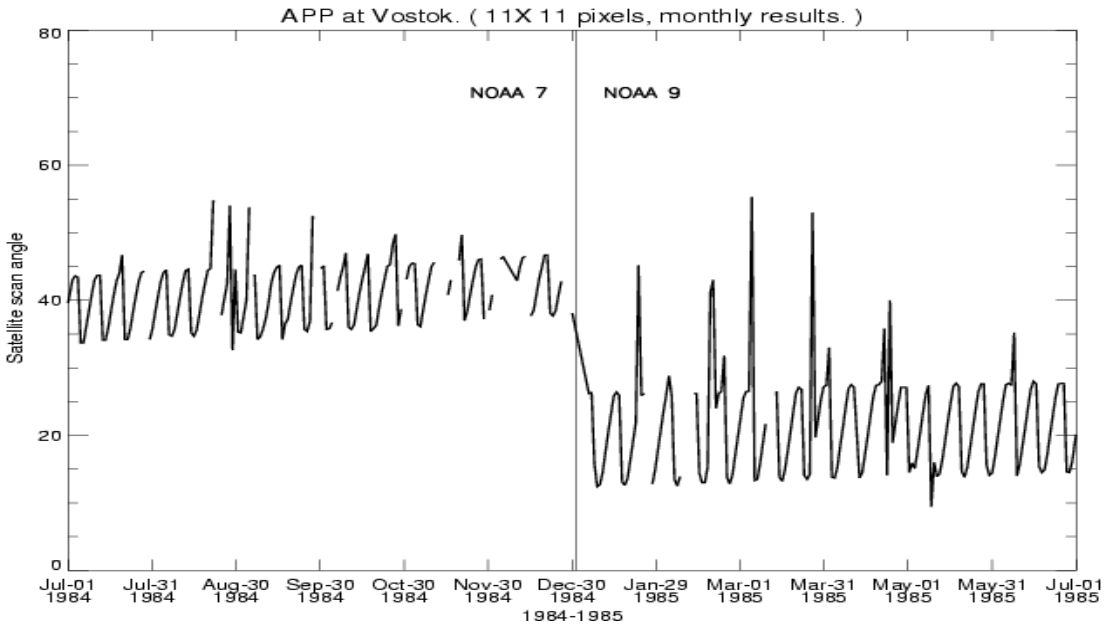

Figure 14: Time series of the AVHRR scan angle averaged over a 275 x 275 km^2 area around Vostok, Antarctica from July 1, 1984 to July 1, 1985 at a local solar time of 1400, covering the transition of NOAA-7 to NOAA-9.

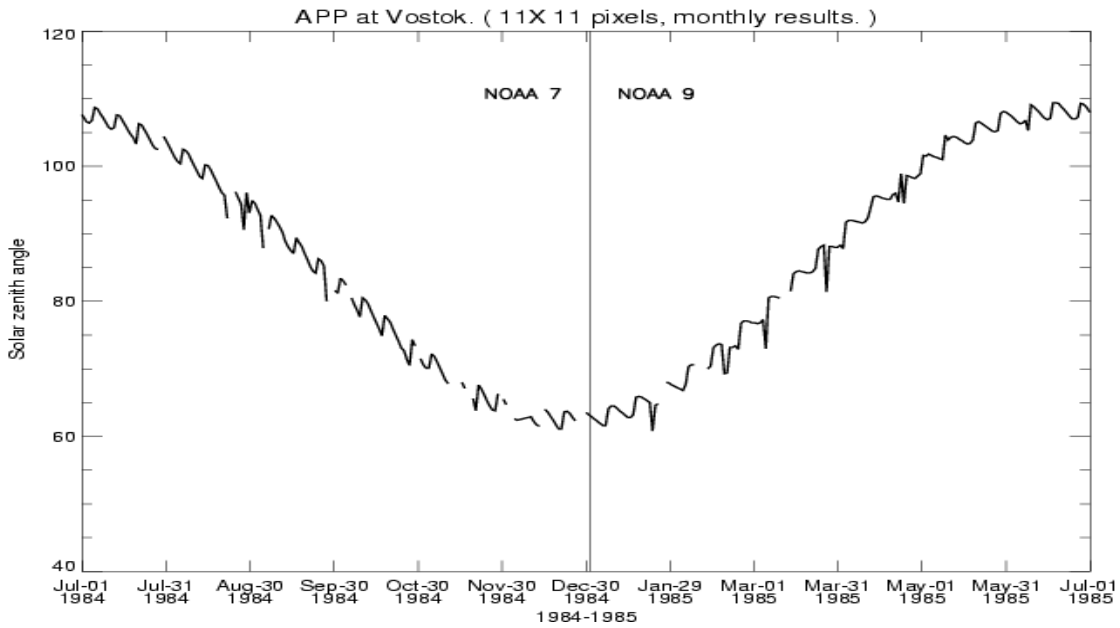

Figure 15: Time series of the solar zenith angles averaged over a 275 x 275 km^2 area around Vostok, Antarctica from July 1, 1984 to July 1, 1985 at local solar time of 1400, covering the transition from NOAA-7 to NOAA-9.

The differences of APP v1.0 and v2.0 are manifested in the differences of the visible channel reflectance. The mean visible channel reflectance difference on some days can be as high as around 3%, with higher differences on individual grids; the infrared channel brightness temperature differences are negligible. Figure 16 show an example of the differences of reflectance differences of Channel 2, and brightness temperature differences of Channel 4 on July 15, 2016.

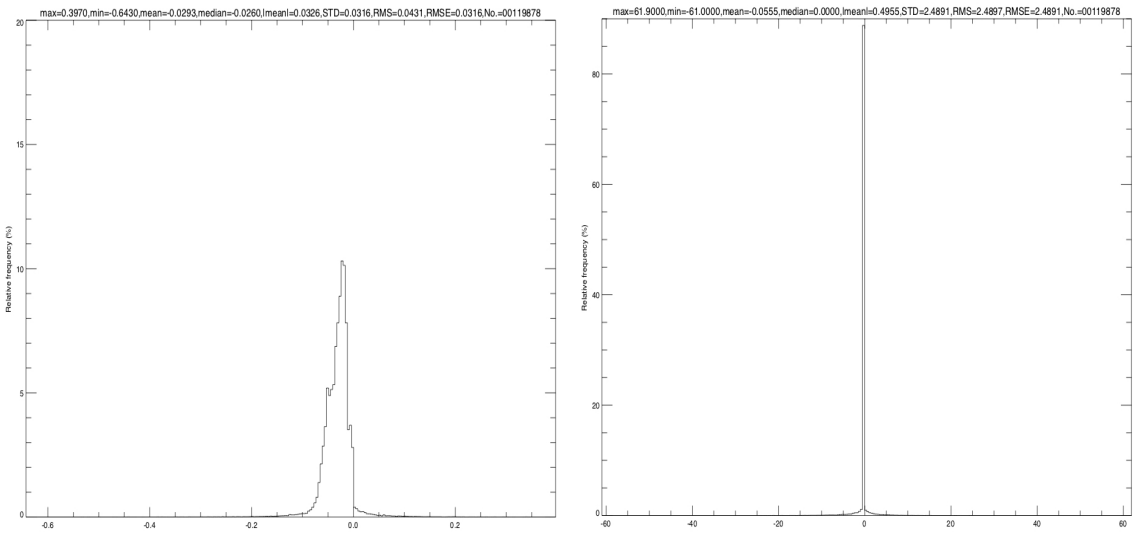

Figure 16: Histogram of Channel 2 reflectance differences (left), and Channel 4 brightness temperature differences at local solar time of 1400 on July 15, 2016.

6.2 Sensor Performance

Degradation of the AVHRR visible channel is addressed explicitly in the reflectance channel calibration method employed here. Thermal channels have on-board calibration so sensor degradation is not an issue.

7. Future Enhancements

7.1 Enhancement 1

Currently, the quality assessment and diagnostics are done by checking the quality of the Advanced AVHRR Polar Pathfinder dataset (APP-x), which derives higher-level geophysical parameters from the APP product. Quality assessment and diagnostics specific to APP are being designed and will be implemented in the future. The quality assessment approach includes automatic daily composite display and monitoring of time series of variables derived in APP-x.

8. References

Cavalieri, D. J., P. Gloersen, and H. Zwally. Edited by J. Maslanik and J. Stroeve, 1999, Near-Real-Time DMSP SSMIS Daily Polar Gridded Brightness Temperatures. Boulder, Colorado USA: NASA National Snow and Ice Data Center Distributed Active Archive Center. http://dx.doi.org/10.5067/AKQDND71ZDLF.

Foster, J.M., and A. Heidinger, 2013, PATMOS-x: Results from a diurnally corrected 30-year satellite cloud climatology. Journal of Climate, Volume 28, Issue 2, pp. 414-425.

Goodison, B. E. ,1989, Determination of Areal Snow Water Equivalent on the Canadian Prairies Using Passive Microwave Satellite Data. IGARSS '89 Proceedings 3:1243-1246.

Heidinger, A.K., W.C. Straka III, C.C. Molling, J.T. Sullivan, and X. Wu, 2010, Deriving an inter-sensor consistent calibration for the AVHRR solar reflectance data record. International Journal of Remote Sensing, Volume 31, Issue 24, pp. 6493-6517.

Heidinger, A. K. et al., 2002, Using Moderate Resolution Imaging Spectrometer (MODIS) to calibrate Advanced Very High Resolution Radiometer reflectance channels. Journal of Geophysical Research. Vol. 107. doi: 10.1029/2001JD002035.

Key, J. R., and J. M. Intrieri, 2000, Cloud particle phase determination with the AVHRR, J. Appl. Meteorol., 39, 1797– 1804.

Key, J. R., X. Wang, J. C. Stoeve, and C. Fowler, 2001, Estimating the cloudy-sky albedo of sea ice and snow from space, J. Geophys. Res., 106, 12,489– 12,497, doi:10.1029/2001JD900069.

Key, J., P. Yang, B. Baum, and S. Nasiri, 2002, Parameterization of shortwave ice cloud optical properties for various particle habits, J. Geophys. Res., 107(D13), 4181, doi:10.1029/2001JD000742.

Kidwell, Katherine B., comp. and ed., 1995, NOAA Polar Orbiter Data (TIROS-N, NOAA-6, NOAA-7, NOAA-8, NOAA-9, NOAA-10, NOAA-11, NOAA-12, and NOAA-14) Users Guide: Washington, D.C., NOAA/NESDIS, http://www.ncdc.noaa.gov/oa/pod-guide/ncdc/docs/podug/.

Kidwell, Katherine B., comp. and ed., 2009, NOAA KLM User's Guide with NOAA-N, -P Supplement (February 2009 Revisions), http://www.ncdc.noaa.gov/oa/pod-guide/ncdc/docs/klm/index.htm.

Liu, Y., J. R. Key, and X. Wang, 2008, The influence of changes in cloud cover on recent surface temperature trends in the Arctic, J. Clim., 21, 705– 715, doi:10.1175/2007JCLI1681.1.

Molling, C.C., A.K. Heidinger, W.C. Straka III, and X. Wu, 2010, Calibrations for AVHRR channels 1 and 2: review and path towards consensus. International Journal of Remote Sensing, 31:6519 - 6540.

Nolin, A. W., R. Armstrong, and J. Maslanik. 1998. Near-Real-Time SSM/I-SSMIS EASE Grid Daily Global Ice Concentration and Snow Extent. Version 4. Boulder, Colorado USA: NASA DAAC at the National Snow and Ice Data Center.

Robel, J., Ed., 2009, NOAA KLM User's Guide with NOAA-N, -N0 Supplement. Available online at: http://www.ncdc.noaa.gov/oa/pod-guide/ncdc/docs/intro.htm

Sullivan, J. and Jelenak, A., 2007, Correcting Geo-Location Interpolation Errors in Nesdis-Produced AVHRR 1b Data near the Poles. International Journal of Remote Sensing, 28(16), 3721-3728. [10.1080/01431160701313818]

Trischenko, A. P., G. Fedosejevs, Z. Li, and J. Cihlar, 2002, Trends and uncertainties in thermal calibration of AVHRR radiometers onboard NOAA-9 to -16, J. Geophys. Res., 107(D24), 4778, doi:10.1029/2002JD002353.

Wang, X. J., and J. R. Key, 2003, Recent trends in arctic surface, cloud, and radiation properties from space, Science, 299, 1725 – 1728, doi:10.1126/science.1078065.

Wang, X. J., and J. R. Key, 2005a, Arctic surface, cloud, and radiation properties based on the AVHRR Polar Pathfinder dataset. Part I: Spatial and temporal characteristics, J. Clim., 18, 2558 – 2574, doi:10.1175/JCLI3438.1.

Wang, X. J., and J. R. Key, 2005b, Arctic surface, cloud, and radiation properties based on the AVHRR Polar Pathfinder dataset. Part II: Recent trends, J. Clim., 18, 2575– 2593, doi:10.1175/JCLI3439.1.

Appendix A. Acronyms and Abbreviations

Acronym or Abbreviation	Meaning
APP	AVHRR Polar Pathfinder
APP-x	eXtended AVHRR Polar Pathfinder (APP)
AVHRR	Advanced Very High Resolution Radiometer
C-ATBD	Climate Algorithm Theoretical Basis Document
CDR	Climate Data Record
CIMSS	Cooperative Institute for Meteorological Satellite Studies, University of Wisconsin-Madison
EASE	Equal-Area Scalable Earth
EUMETSAT	European Organization for the Exploitation of Meteorological Satellites
ESA	European Space Agency
GAC	Global Area Coverage
IDL	Interactive Data Language
MODIS	Moderate-resolution Imaging Spectroradiometer
NASA	National Aeronautics and Space Administration
NCDC	National Climatic Data Center
NCEI	National Centers for Environmental Information
NCEP	National Centers for Environmental Prediction
NESDIS	NOAA's Satellite and Information Service
NOAA	National Oceanic and Atmospheric Administration
NSIDC	National Snow and Ice Data Center
SSEC	Space Science and Engineering Center, University of Wisconsin-Madison
STAR	The Center for Satellite Applications and Research
UW-Madison	University of Wisconsin-Madison
VGAC	VIIRS Global Area Coverage
VPP	VIIRS Polar Pathfinder

Appendix B. Coefficients for Calibration of VIIRS Channels to NOAA-19 AVHRR Channels

The coefficients of a_0, a_1, a_2, a_3, a_4

Channel			Arctic		Antarctica	
AVHRR	VIIRS	Coefficient	Local Solar Time (LST)		Local Solar Time (LST)	
			14:00	04:00	14:00	02:00
Channel 1	I 1	a_0	0.0279289	0.140671	0.0866695	0.236379
		a_1	0.958457	0.876844	0.889131	0.757802
		a_2	2.29427e-5	-6.14374e-5	0.00180543	2.56999e-5
		a_3	-0.000377165	-0.00135043	-0.00129548	-0.00272291
		a_4	-1.18182e-5	-0.000331505	4.73859e-5	-3.36418e-6
Channel 2	I 2	a_0	0.0115684	0.114859	-0.0306988	0.185096
		a_1	0.911808	0.828645	0.901164	0.764386
		a_2	-0.000148943	-8.58867e-5	0.0025043	6.09533e-5
		a_3	-0.000108634	-0.00091091	-0.000786054	-0.00209245
		a_4	-1.69862e-5	-0.000449429	0.00108355	2.67030e-6
Channel 3b	M 12	a_0	1.69724	-6.7134	-29.8107	-8.899975
		a_1	1.00030	1.02721	1.09861	1.03651
		a_2	0.00631131	-0.0198463	0.0326141	0.0134049
		a_3	-0.0304901	-0.0141215	0.0373118	-0.00884032
		a_4	-0.0016342	0.0139979	0.00317988	-0.00690353
Channel 4	M 15	a_0	6.93539	0.698029	-0.458771	3.14281
		a_1	0.97695	0.99542	1.00103	0.988042
		a_2	0.00570868	0.00804077	0.0409503	0.0125797
		a_3	-0.0126428	0.00338759	-0.015331	-0.0025922
		a_4	-0.000226796	0.00221654	0.0206819	-0.00055987
Channel 5	M 16	a_0	9.59573	2.96457	-1.25966	3.95871
		a_1	0.966319	0.986297	1.00119	0.984118
		a_2	0.00532354	0.00518083	0.0421954	0.0122486
		a_3	-0.0147809	0.0019786	-0.0152040	-0.00380756
		a_4	-0.000722889	0.00212637	0.0289954	-0.000109788